Proceedings of the 45th IEEE Conference on Decision & Control
Manchester Grand Hyatt Hotel
San Diego, CA, USA, December 13-15, 2006



# Constrained motion planning for the airpath of a Diesel HCCI engine

Jonathan Chauvin, Gilles Corde, and Nicolas Petit

*Abstract*— **A constrained motion planning control strategy is proposed for the airpath control of turbocharged Diesel engines using exhaust gas recirculation (EGR). The considered model uses simple balance equations. The fully actuated dynamics are easily inverted, yielding straightforward open-loop control laws. Yet, practical constraints need to be accounted for. Convergence is proven and stress that saturation of infeasible control values yields longer yet successful transients. This fact is supported by reported extensive experimental tests on a 4-cylinder engine in Homogeneous Charge Compression Ignition (HCCI) mode. Conclusions stress the possibility of taking into account the non-minimum phase effects of this system by a simple, yet efficient and realistic in practice, control law.**

## I. Introduction

Performance and environmental requirements of Diesel engines have steadily increased over the last thirty years, which in turn has required an increase in the sophistication of employed control strategies. Advances in model based control over this period have been one of the keys in meeting the demands placed on modern combustion technologies. Lately, the Highly Premixed Combustion mode (HPC) – including Homogeneous Charge Compression Ignition (HCCI) – has become of major interest. It requires the use of high Exhaust Gas Recirculation (EGR) rates. The key idea is that the recirculated burned gas lower the in-cylinder temperature and dilute the air charge which reduces the emissions of nitrogen oxides. Simultaneous ignition in the whole combustion chamber is performed and controlled. Significant reduction in pollutants emission was proven in practice through numerous experiments (see [14], [8], [21], [3] for example). In that combustion mode, the core variable is the Burned Gas Rate (BGR) in the intake manifold (see Figure 1). BGR Offsets may cause misfires and malicious noises. In the HCCI combustion mode it is very high ($40\%$ or more). Accurate control of BGR can be achieved by controlling the whole airpath system: intake and exhaust manifolds, EGR loop and fresh air loop. This is the subject of the paper.

As studied in [16], [15], the airpath system of a turbocharged Diesel engine features coupled dynamics. The EGR acts as a discharge valve for the turbocharger. Most studies consider the following control setup: both intake pressure and intake air flow are closely controlled using EGR valve and Variable Geometry Turbocharger (VGT) using Gain schedulling PI controllers as in [20], [18], [19], using constructive Lyapunov control as in [10], [11] or LPV formulation as in [12], [13]. Controlling both intake and exhaust pressure has been exposed in [2]. All these studies prove the relevance of a multivariable control. Following a preliminary approach we presented in [5], we use a motion planning strategy by expliciting a feed-forward term. Originally, our objective is to satisfy the drivers's torque demand. Successively, we cast it into in-cylinder masses setpoint, then into BGR and intake manifold pressure control problem. Then, an explicit unconstrained transient is computed. Hopefully, thanks to tuning parameters, it is consistent with physically important constraints on the inputs. If not, it is saturated, and, as is proven, eventually provides convergence anyway.

The contribution of the paper is as follows. Constraints are explicitly accounted for, convergence analysis is performed, and extensive experimental results are reported. At the light of this study, we can finally conclude, with supportive results, that motion planning is indeed an appropriate solution for controlling the airpath dynamics.

The paper is organized as follows. In Section II, we detail the control problem. In Section III, we decouple the airpath fully actuated dynamics by a simple motion planning strategy. Physical input constraints are explicited in the motion planning strategy. In Section IV, we detail a convergence analysis. It provides a tuning methodology. Experimental results are reported on a $4$ cylinder HCCI engine in Section V. Conclusions and future directions are given in Section VI.

## II. Control Problem

Our approach to combustion control is to manage the air and burned gas masses in the cylinder. In other words, we focus on the airpath system. Figure 1 shows the flow sheet of the airpath. Flows of fresh air and the Exhaust Gas Recirculation (EGR) mix into the intake manifold and are aspirated into the cylinders.

Engine control performance requirements usually include consumption, pollutants, and noise reduction. Those requirements are often incompatible. Therefore, a tradeoff is needed. This impacts the reference setpoints of air and burned gas masses in the cylinder ($M_{air,cyl}$ and $M_{bg,cyl}$). In practical applications, those variables can not be measured. Yet, equivalent variables can be considered. Controlling those two masses is equivalent to controlling the intake pressure $P_{int}$ (being an image of $M_{air,cyl} + M_{bg,cyl}$) and the burned gas rate $F_{int}$ (representing $\frac{M_{bg,cyl}}{M_{air,cyl}+M_{bg,cyl}}$). Setpoints are

J. Chauvin (corresponding author) is a PhD Candidate in Mathematics and Control, Centre Automatique et Systèmes, École des Mines de Paris, 60, bd St Michel, 75272 Paris, France chauvin@cas.ensmp.fr.

G. Corde is with the Department of Engine Control in Institut Français du Pétrole, 1 et 4 Avenue de Bois Préau, 92852 Rueil Malmaison, France

N. Petit is with the Centre Automatique et Systèmes, École des Mines de Paris, 60, bd St Michel, 75272 Paris, France

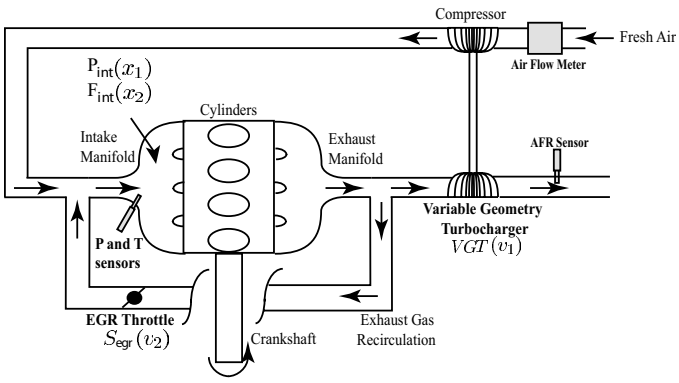


Fig. 1. Air path problem. The sensors used are colored in grey.

TABLE I

NOMENCLATURE. I.M. REFERS TO THE INTAKE MANIFOLD.

| Var. | Quantity | Unit | Symb. |
|---|---|---|---|
| $P_{int}$ | Pressure in the i.m. | Pa | $x_1$ |
| $F_{int}$ | BGR: Fraction of burned gas in the i.m. | - | $x_2$ |
| $\eta_{vol}$ | Volumetric efficiency | - | |
| $\alpha_{int}$ | Parameter | | |
| $\beta_{int}$ | Parameter | | |
| $D_{air}$ | Manifold air flow | kg.s$^{-1}$ | $u_1$ |
| $D_{egr}$ | EGR flow | kg.s$^{-1}$ | $u_2$ |
| $T_{int}$ | Temperature in the i.m. | K | |
| $N_e$ | Engine Speed | rpm | |
| $F_{exh}$ | Fraction of burned gas in the exhaust mamifold | - | |
| $S_{\text{VGT}}$ | VGT normalized position | - | $v_1$ |
| $S_{\text{egr}}$ | EGR valve effective area | - | $v_2$ |
| $u_{min}$ | Constraint parameter | - | |

often chosen to maximize EGR in order to lower the $NO_x$ emissions at low load. At high load, the negative impact of EGR onto combustion stability and efficiency imposes the use of low EGR. Typically, the setpoint at 1500 rpm and high load is $(P_{int,sp} = 2\text{bar},\ F_{int,sp} = .05)$ using low EGR, while at 1500 rpm and low load setpoints under consideration are close to $(P_{int,sp} = 1.013\text{bar},\ F_{int,sp} = .45)$ using high EGR.

In this context, the control problem we need to address is a large transient problem for a two outputs, two inputs system. The control inputs are the VGT actuator position $S_{vgt}(v_1)$ (ranging from 0 to 1) and the EGR valve normalized effective area $S_{egr}(v_2)$ (ranging from 0 to 1). Both are bounded. Other external inputs include the fueling rate and the engine speed $N_e$. The underlying dynamics is also of dimension 2. The states are the outputs: $P_{int}$ and $F_{int}$.

The intake manifold dynamics can be quite accurately represented, *at a low time resolution ($180^o$ TDC time scale)*, using mass balances. Several key assumptions need to be considered. We assume the gas to be ideal and we neglect high frequency aspiration phenomena. Finally, assuming slow intake temperature variation, mass balance and mixing dynamics write under the form

$$\left\{ \begin{array}{rcl} \dot{x}_1 & = & \alpha_{int}\left(u_1 + u_2 - \eta_{vol}(x_1, N_e)\beta_{int}x_1\right) \\ \dot{x}_2 & = & \frac{\alpha_{int}}{x_1}\left(F_{exh}u_2 - (u_1+u_2)x_2\right) \end{array} \right. \quad (1)$$

A nomenclature is given in Table I.

In these equations, $\eta_{vol}$ is the volumetric efficiency which is experimentally derived and defined though a look-up table. It is bounded by $\underline{\eta_{vol}} = .7$ and $\overline{\eta_{vol}} = 1$. Also, note that the *strictly positive* parameters $\alpha_{int}$ and $\beta_{int}$ are computed through available measurements and engine characteristics.

$$\alpha_{int} \triangleq \frac{RT_{int}}{V_{int}} \quad \text{and} \quad \beta_{int} \triangleq \frac{1}{RT_{int}} V_{cyl} \frac{N_e}{120}$$

More details about this model can be found in [5], [6].

## III. MOTION PLANNING

As will be proven next, system (1) is open-loop asymptotically stable. Yet, using (appropriately valued) step inputs does not provide satisfactory transients. It has been impossible for us to get such a control strategy to work

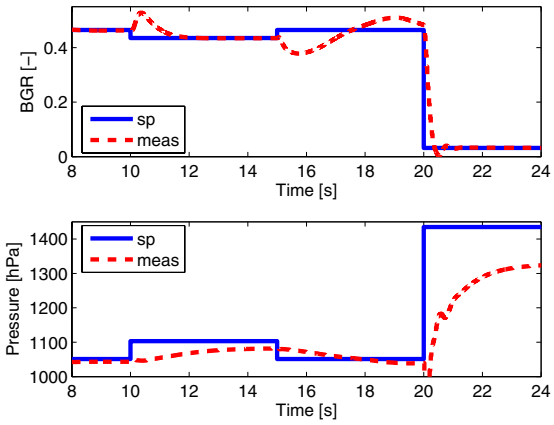


Fig. 2. Tentative open loop transients with step inputs.

efficiently on our test bench. Numerical simulations through the AMESIM environment (see Section V-A for details) have provided us with some insights. In Figure 2, it appears that without model-based feedforward action, one is not able to take into account the apparent non-minimum phase effect of dynamics (1). There are too many oscillations and too large errors. These can not be damped before a new transient is to be achieved.

On the other hand, it also appears that interaction between air and EGR loops combined with the nonlinear nature of the system between highly varying setpoints makes the system difficult to handle using classical control design methods. We propose a motion planning control strategy which rely on the computation of transient trajectories for the airpath dynamics (1). This strategy is detailed in Figure 3. It comprises 4 sub procedures: setpoint computations through static maps (first two blocks in Figure 3), trajectory generation, model inversion, and saturation of open-loop control values. We now detail these in the next Section, we actually prove the convergence of the airpath system when using this strategy.

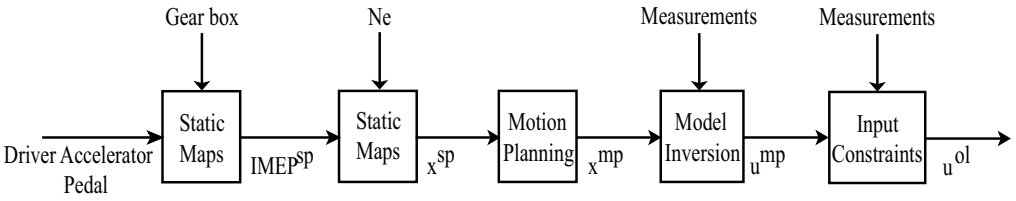


Fig. 3. Motion planning scheme: from torque demand to feedforward control.

### A. Set points

The driver's request considered here is the accelerator position. First, taking into account the gear box configuration, this request is turned into a torque control objective under the form of an IMEP (Indicated Mean Effective Pressure) set point. Then, the set points for the intake pressure and the BGR (noted $x^{\text{sp}}$ in Figure 3) are inversely given by experimentally calibrated static maps on the $(IMEP^{\text{sp}}, N_e)$ operating range. The engine speed $N_e$ is not modelled but directly measured. The $x^{\text{sp}} = (x_1^{\text{sp}}, x_2^{\text{sp}})$ vector is defined as

$$\begin{array}{rcl} x_1^{\text{sp}} & = & f_{\text{pressure}}(IMEP^{\text{sp}}, N_e) \\ x_2^{\text{sp}} & = & f_{\text{bgr}}(IMEP^{\text{sp}}, N_e) \end{array}$$

### B. Motion planning

Because $IMEP^{\text{sp}}$ is arbitrarily specified by the driver, $t \mapsto x_1^{\text{sp}}(t)$ and $t \mapsto x_2^{\text{sp}}(t)$ may not be smooth nor monotonous. These signals must be filtered to correspond to feasible trajectories of (1). This can be done by many methods. Here, we propose the following approach that, among several properties, is easy to handle in the convergence analysis process. It addresses only the case of transients from one steady state to another. From a current steady state $\underline{x}$ to a target $\overline{x}$ we use an interpolation formula. Coordinate wise this defines $x_1^{\text{mp}}$ and $x_2^{\text{mp}}$. Let

$$\phi(t,T) = \left\{ \begin{array}{cc} 0 & \text{for } \ 0 \geq t \\ (\frac{t}{T})^2(3-2\frac{t}{T}) & \text{for } \ 0 \leq t \leq T \\ 1 & \text{for } \ T \leq t \end{array} \right. \qquad (2)$$

Note two positive constants $T_1$ and $T_2$. The considered interpolation is

$$\left\{ \begin{array}{rcl} x_1^{\text{mp}}(t) & = & \underline{x}_1 + (\overline{x}_1 - \underline{x}_1)\phi(t,T_1) \\ x_2^{\text{mp}}(t) & = & \underline{x}_2 + (\overline{x}_2 - \underline{x}_2)\phi(t,T_2) \end{array} \right. \qquad (3)$$

### C. Model inversion

System (1) is fully actuated and invertible. Thus, an analytic expression of the input can be derived from the state variables and their first derivatives histories. In fact,

$$\left\{ \begin{array}{l} u_1 + u_2 = \eta_{vol}(x_1, N_e)\beta_{int}x_1 + \frac{1}{\alpha_{int}}\dot{x}_1 \\ -x_2u_1 + (F_{exh} - x_2)u_2 = \frac{1}{\alpha_{int}}\dot{x}_2x_1 \end{array} \right. \qquad (4)$$

This rewrites

$$\left\{ \begin{array}{rcl} u_1 & = & f_1(x, \dot{x}) \\ u_2 & = & f_2(x, \dot{x}) \end{array} \right. \qquad (5)$$

with

$$\left\{ \begin{array}{rcl} f_1(x,\dot{x}) & = & \frac{1}{F_{exh}}\Big(\frac{F_{exh}-x_2}{\alpha_{int}}\dot{x}_1 - \frac{1}{\alpha_{int}}\dot{x}_2x_1 \\ & & \quad +(F_{exh} - x_2)\eta_{\text{vol}}(x_1, N_e)\beta_{int}x_1\Big) \\ f_2(x,\dot{x}) & = & \frac{1}{F_{exh}}\Big(\frac{1}{\alpha_{int}}x_2\dot{x}_1 + \eta_{\text{vol}}(x_1, N_e)\beta_{int}x_2x_1 \\ & & \quad +\frac{1}{\alpha_{int}}\dot{x}_2x_1\Big) \end{array} \right. \qquad (6)$$

In these last expressions, $F_{\text{exh}}$, $\alpha_{int}$, $N_e$, and $\beta_{int}$ are all given by sensors measurements. The unique open-loop control law $(u_1^{\text{mp}}, u_2^{\text{mp}})$ corresponding to any desired $(x_1^{\text{mp}}, x_2^{\text{mp}})$ trajectory (defined by formulas (3)) is

$$\left\{ \begin{array}{rcl} u_1^{\text{mp}} & = & f_1(x_1^{\text{mp}}, \dot{x}_1^{\text{mp}}, x_2^{\text{mp}}, \dot{x}_2^{\text{mp}}) \\ u_2^{\text{mp}} & = & f_2(x_1^{\text{mp}}, \dot{x}_1^{\text{mp}}, x_2^{\text{mp}}, \dot{x}_2^{\text{mp}}) \end{array} \right. \qquad (7)$$

### D. Input constraints

There are several constraints that need to be considered. Input signals $(u_1, u_2)$ and the aspirated flow $(u_1 + u_2)$ must be positive and strictly positive, respectively, because they correspond to input flows. Also, the inputs must not cause misfires (usually due to high EGR). A simple strategy can address this issue. Conservatively, misfire avoidance can be guaranteed provided the following input constraints are satisfied

$$C(u) \triangleq F_{exh}\frac{u_2}{u_2 + u_1} \leq \overline{C} < 1$$

Adding the previously discussed positiveness of input flows, the set of admissible inputs is defined as

$$\begin{array}{rl} \mathcal{U} \triangleq & \big\{(u_1,u_2) \in (\mathbb{R})^2 / u_1 + u_2 \geq u_{min}, \quad u_2 \geq 0, \\ & \qquad \text{and } F_{exh}\frac{u_2}{u_2+u_1} \leq \overline{C}\big\} \end{array}$$

and we note $\partial\mathcal{U}$ its boundary. We define the constrained control as

$$u^{\text{ol}}(t) \triangleq arg(\min_{u \in \mathcal{U}} \ (u_1 - u_1^{\text{mp}}(t))^2 + (u_2 - u_2^{\text{mp}}(t))^2) \quad (8)$$

where $u_1^{\text{mp}}(t)$ and $u_2^{\text{mp}}(t)$ are defined by (7). In other words, for all $t \in \mathbb{R}^+$, $u^{\text{ol}}(t)$ is the projection of $u^{\text{mp}}(t) = (u_1^{\text{mp}}, u_2^{\text{mp}})(t)$ on to the set $\mathcal{U}$. In (8), both the cost function and the admissible set $\mathcal{U}$ are convex. Thus, there always exists a uniquely defined solution $x^{\text{ol}}$. In fact, this solution can be analytically, computed in a straightforward way (by enumerating 6 possible solutions), which is compatible with our real-time control application requirements.

## IV. Convergence and tuning of the constrained motion planning

We now prove that the proposed control strategy actually converges. The main focus is on the impact of input saturations as defined in Section III-D.

It is assumed that the volumetric efficiency slowly varies w.r.t. the intake pressure $x_1$. Denoting $h(x_1, N_e) \triangleq \eta_{vol}(x_1, N_e)x_1$, we suppose that there exists a strictly positive constant $\bar{h}$ such that for all $(x_1, N_e)$ in $\mathbb{R}^+ \times [500, 4500]$,

$$\frac{\partial h}{\partial x_1}(x_1, N_e) \geq \bar{h} > 0$$

Experimentally, this assumption is actually easy to validate.

### A. Exponential stability

Stability can be studied by exploiting the cascade structure of equations (1). Imposing a constant input $u = \bar{u} \in \mathcal{U}$, the dynamics writes

$$\left\{ \begin{array}{rcl} \dot{x}_1 & = & \alpha_{int}(\bar{u}_1 + \bar{u}_2 - h(x_1, N_e)) \\ \dot{x}_2 & = & \frac{\alpha_{int}}{x_1}(F_{exh}\bar{u}_2 - (\bar{u}_1 + \bar{u}_2)x_2) \end{array} \right.$$

Yet, $h$ is a strictly increasing function w. r. t. $x_1$ over $\mathbb{R}^+$ with $h(0) = 0$. Since $\bar{u} \in \mathcal{U}$, then $\bar{u}_1 + \bar{u}_2 \geq u_{min} > 0$. Thus, there exists a unique $z_1 \in \mathbb{R}^+ \backslash \{0\}$ such that $h(z_1, N_e) = \bar{u}_1 + \bar{u}_2$. Since $\frac{\partial h}{\partial x_1}(z_1, N_e) \geq \bar{h} > 0$, we can conclude that $x_1$ exponentially converges toward $z_1$. Further, $z_1$ is strictly positive. Thus, for any positive initial condition, exponential convergence guarantees that there exist two positive constants $(x_m, x_M)$ such that for all $t \in \mathbb{R}^+$, $x_M \geq x_1(t) \geq x_m > 0$.

Now, we focus on the second equation. We notice that $\bar{u}_1 + \bar{u}_2 \geq u_{min} > 0$ and $0 < \frac{\alpha_{int}}{x_M} \leq \frac{\alpha_{int}}{x_1} \leq \frac{\alpha_{int}}{x_m}$. This imply that $x_2$ exponentially converges toward $z_2 = F_{exh}\frac{\bar{u}_2}{\bar{u}_1+\bar{u}_2}$. As a consequence, for every constant input, the system exponentially converges toward $z = (z_1, z_2)$.

Conversely, it is possible to tune the input values to reach a desired set point $\bar{x} = (\bar{x}_1, \bar{x}_2)$. For that purpose, one should use

$$\left\{ \begin{array}{rcl} \bar{u}_1 & = & \frac{F_{exh}-\bar{x}_2}{F_{exh}}\eta_{\text{vol}}(\bar{x}_1, N_e)\beta_{int}\bar{x}_1 \\ \bar{u}_2 & = & \frac{1}{F_{exh}}\eta_{\text{vol}}(\bar{x}_1, N_e)\beta_{int}\bar{x}_1\bar{x}_2 \end{array} \right. \quad (9)$$

*Proposition 1:* Consider system (1). For any constant input $u = (\bar{u}_1, \bar{u}_2)$, the state $x$ exponentially converges toward $z \triangleq (z_1, z_2)$ where $h(z_1, N_e) = \bar{u}_1 + \bar{u}_2$ and $z_2 = F_{exh}\frac{\bar{u}_2}{\bar{u}_1+\bar{u}_2}$. A way to asymptotically reach $\bar{x} = (\bar{x}_1, \bar{x}_2)$ is to use a constant input $\bar{u}$ as defined in (9).

This proposition is the key to understanding our approach. Provided chosen control values are feasible (i.e. belong to $\mathcal{U}$), it is sufficient to use them as the step inputs in the airpath system to asymptotically reach the desired set point. Now, as we mentioned it in the Introduction, our goal is to provide more efficient transients. Ideally, we would like to have soft landing and fast transient. If the proposed control (7) are feasible, then $u^{\text{mp}}(t) = u^{\text{ol}}(t)$ for all $t \in \mathbb{R}^+$ and, neglecting possible perturbations, the transient is perfectly achieved. Yet, if the motion planning strategy is, at times, inconsistent with the input constraints, then $u^{\text{mp}}(t) \neq u^{\text{ol}}(t)$ during the transient. In any cases, for large values of $t$ ($t \geq \max\{T_1, T_2\}$ as used in (2)), both coincide again and equal the feasible final input values. Ultimately, the system converges. The motion planning strategy can only improve transients when the computed input values are feasible, at least over some reasonably long period of the transient interval.

We now perform some analysis that allows us to guarantee this desired feasibility. From this, we can derive guidelines to tune parameters $T_1$ and $T_2$.

### B. Transient tuning

Our open loop trajectories (3) are defined by two parameters: $T_1$ and $T_2$. Certainly, this is a rather rough description of possible manoeuvers. Further developments could include the definition of the interpolation function $\phi$ by B-splines functions as in [17]. What motivates this restrictive choice is again the requirements of our real-time control system running at $100Hz$ at 1500rpm and the *relatively* heavy computational burden implied by this other approach.

We first show that for large enough values for $T_1$ and $T_2$, the control values do not violate the constraints. Then, we explain why it is possible to reduce $T_2$, once $T_1$ has been chosen.

For $t \in [0, T]$, the derivative of $\phi(., T)$ (defined in (2)) writes $\frac{d\phi}{dt}(t, T) = \frac{6}{T}\frac{t}{T}(1 - \frac{t}{T})$. Its maximum is reached at $t = \frac{T}{2}$ and its value is $\frac{3}{2T}$.

Consider a transient defined between the setpoints $(\underline{x}, \underline{u})$ and $(\overline{x}, \overline{u})$. Assume that $(\underline{u}, \bar{u}) \in \mathcal{U}^2$. We will show that for large enough $T_1$ and $T_2$, the motion planning control defined in (5) satisfies $u^{\text{mp}}(t) \in \mathcal{U}$ for all $t \in \mathbb{R}^+$.

The function (2) is monotonous. It gives a monotonous $t \mapsto x_1^{\text{mp}}(t)$. For $\epsilon > 0$, we denote

$$T_{M,1}(\epsilon) \triangleq \frac{2}{\epsilon}\frac{|\overline{x}_1 - \underline{x}_1|}{\alpha_{int}} \quad (10)$$

Then, we have for all $t \in \mathbb{R}^+$

$$\left| \frac{\dot{x}_1^{\text{mp}}(t)}{\alpha_{int}} \right| \leq \left| \frac{\dot{x}_1^{\text{mp}}(\frac{T_{M,1}}{2})}{\alpha_{int}} \right| \leq \frac{3\,|\overline{x}_1 - \underline{x}_1|}{2T_{M,1}\alpha_{int}} < \epsilon$$

and, from (7)

$$-\epsilon < (u_1^{\text{mp}} + u_2^{\text{mp}})(t) - \beta_{int}h(x_1^{\text{mp}}(t), N_e) < \epsilon$$

Further, $h$ is monotonous w.r.t. $x_1$. It follows that $t \mapsto h(x_1^{\text{mp}}(t), N_e)$ is monotonous w.r.t. t. Thus,

$$(u_1^{\text{mp}} + u_2^{\text{mp}})(t) \geq \min\{\underline{u}_1 + \underline{u}_2, \bar{u}_1 + \bar{u}_2\} - \epsilon > 0 \quad (11)$$

Let $\epsilon_1 \triangleq \min\{\underline{u}_1 + \underline{u}_2, \bar{u}_1 + \bar{u}_2\} - u_{min} \geq 0$. If $\epsilon_1 > 0$, i.e. $(\underline{u}, \bar{u}) \in (\mathcal{U} \backslash \partial\mathcal{U})^2$, then by choosing $T_1 > T_{M,1}(\frac{\epsilon_1}{2})$ we have for all $t \in \mathbb{R}^+$,

$$(u_1^{\text{mp}} + u_2^{\text{mp}})(t) > u_{min}$$

Under this assumption, $u_2 \geq 0$ is equivalent to $C(u) \geq 0$. Along the planned trajectory, using (7), the constraint $C$ writes

$$C(u^{\text{mp}}(t)) = x_2^{\text{mp}}(t) + \frac{\dot{x}_2^{\text{mp}}(t)}{p_{T_1}(t)}$$

where

$$p_{T_1}(t) \triangleq \frac{\dot{x}_1^{\text{mp}}(t)}{x_1^{\text{mp}}(t)} + \Phi_{\text{int}}\eta_{vol}(x_1^{\text{mp}}(t), N_e)$$

and $\Phi_{\text{int}} \triangleq \alpha_{\text{int}}\beta_{\text{int}}$. Notice that the two steady states values satisfy

$$C(\underline{u}) = \underline{x}_2, \quad C(\bar{u}) = \bar{x}_2$$

Then, we have for all $t \in \mathbb{R}^+$

$$\Phi_{int}\underline{\eta_{vol}} - \frac{3\,|\overline{x}_1 - \underline{x}_1|}{2T_1 \min\{\overline{x}_1, \underline{x}_1\}} \leq p_{T_1}(t) \leq \Phi_{int}\overline{\eta_{vol}} + \frac{3\,|\overline{x}_1 - \underline{x}_1|}{2T_1 \min\{\overline{x}_1, \underline{x}_1\}}$$

For the other constraint ($0 \leq C(u) \leq \bar{C}$), we pose, for sufficiently large $T_1$,

$$T_{M,2}(T_1, \epsilon) \triangleq \frac{2}{\epsilon} \frac{|\overline{x}_2 - \underline{x}_2|}{\Phi_{int}\underline{\eta_{vol}} - \frac{3|\overline{x}_1 - \underline{x}_1|}{2T_1 \min\{\overline{x}_1, \underline{x}_1\}}} \tag{12}$$

Thus, if we use $T_2 > T_{M,2}(T_1, \epsilon)$, then we have, for all $t \in \mathbb{R}^+$, $\left|\frac{\dot{x}_2^{\text{mp}}(t)}{p_{T_1}(t)}\right| \leq \epsilon$ and

$$\left|C(u^{\text{mp}}(t)) - x_2^{\text{mp}}(t)\right| \leq \epsilon$$

The motion planning strategy leads to a monotonous $t \mapsto x_2^{\text{mp}}(t)$. That imply that, $\forall t \in \mathbb{R}^+$

$$\begin{cases} C(u^{\text{mp}}(t)) \leq \max\{\underline{x}_2, \bar{x}_2\} + \epsilon \leq \max\{C(\underline{u}), C(\bar{u})\} + \epsilon \\ C(u^{\text{mp}}(t)) \geq \min\{\underline{x}_2, \bar{x}_2\} - \epsilon \geq \min\{C(\underline{u}), C(\bar{u})\} - \epsilon \end{cases}$$

Consider

$$\begin{cases} \epsilon_2^- & \triangleq & \min\{C(\underline{u}), C(\bar{u})\} \geq 0 \\ \epsilon_2^+ & \triangleq & \bar{C} - \max\{C(\underline{u}), C(\bar{u})\} \geq 0 \end{cases}$$

If $\epsilon_2^+ > 0$, i.e. $(\underline{u}, \bar{u}) \in (\mathcal{U}\backslash\partial\mathcal{U})^2$, then by choosing $T_2 > T_{M,2}(T_1, \frac{\epsilon_2^+}{2})$, we have for all $t \in \mathbb{R}^+$, $C(u^{\text{mp}})(t) < \bar{C}$. Similarly, if $\epsilon_2^- > 0$, then by choosing $T_2 > T_{M,2}(T_1, \frac{\epsilon_2^-}{2})$, we have for all $t \in \mathbb{R}^+$, $C(u^{\text{mp}})(t) > 0$ which is equivalent to $u_2^{\text{mp}}(t) > 0$. Thus, if $\epsilon_2 \triangleq \min\{\epsilon_2^-, \epsilon_2^+\} > 0$, for $T_2 > T_{M,2}(T_1, \frac{\epsilon_2}{2})$ we have for all $t \in \mathbb{R}^+$, $u^{\text{mp}}(t) \in \mathcal{U}\backslash\partial\mathcal{U}$ and the following result holds.

*Proposition 2:* Consider the motion planning strategy (7) aiming at steering the system from steady state $(\underline{x}, \underline{u})$ to $(\overline{x}, \overline{u})$. If $(\underline{u}, \bar{u}) \in (\mathcal{U}\backslash\partial\mathcal{U})^2$, then by choosing large enough $T_1$ ($T_1 > T_{M,1}(\frac{\epsilon_1}{2})$) and $T_2$ ($T_2 > T_{M,2}(T_1, \frac{\epsilon_2}{2})$) as constructed above in equations (10) and (12), we have $u^{\text{mp}}(t) \in \mathcal{U}\backslash\partial\mathcal{U}$ for all $t \in \mathbb{R}^+$.

Further, if $\bar{u} \in \partial\mathcal{U}$, then there exist $T_1 > 0$ and $T_2 > 0$ such that the constraints are violated by less than any prescribed $\epsilon$, i.e. the distance $dist(u^{\text{mp}}(t), \mathcal{U}) < \epsilon$ for all $t \in \mathbb{R}^+$.

Now, for a fixed $T_1 \in \mathbb{R}^+$, let us try to reduce $T_2$ until we reach an infeasibility. Note

$$T_m(T_1) \triangleq \frac{|\overline{x}_2 - \underline{x}_2|}{\Phi_{int}\overline{\eta_{vol}} + \frac{3|\overline{x}_1 - \underline{x}_1|}{2T_1 \max\{\overline{x}_1, \underline{x}_1\}}} \tag{13}$$

Then, we have

$$\begin{aligned} \left|\dot{x}_2^{\text{ol}}(\tfrac{T_m(T_1)}{2})\right| &= |\overline{x}_2 - \underline{x}_2| \tfrac{3}{2T_m} \\ &> \max_{t\in[0,T_1]}(p_{T_1}(t)) \\ &> p_{T_1}(\tfrac{T_m(T_1)}{2}) \end{aligned}$$

Thus, for a sufficiently small time $T_2 = T_m(T_1)$, if $\bar{x}_2 > \underline{x}_2$ then $C(u^{\text{mp}}(\frac{T_m(T_1)}{2})) > \bar{C}$, and if $\bar{x}_2 < \underline{x}_2$ then $u_2^{\text{mp}}(\frac{T_m(T_1)}{2}) < 0$ leading to the violation of the constraints, i.e. $u^{\text{mp}}(\frac{T_m(T_1)}{2}) \notin \mathcal{U}$. On the contrary, if $\bar{x}_2 = \underline{x}_2$ we can not necessarily find a time $T_1$ such that the open-loop control strategy violates the constraints (a prime example is $\bar{x}_2 = \underline{x}_2 = 0$ and $\bar{x}_1 > \underline{x}_1$). finally, the following result holds.

*Proposition 3:* If $\bar{x}_2 \neq \underline{x}_2$, for all $T_1 \in \mathbb{R}^+ \setminus \{0\}$, then there exists a time $T_2 = T_m(T_1) > 0$ defined in (13) such that, at least one constraint is always violated by the planned input histories. In facts, $u^{\text{mp}}(\frac{T_m(T_1)}{2}) \notin \mathcal{U}$.

Considering the two presented propositions, we are now able to propose a tuning methodology

1) We choose $\epsilon_1 > 0$ and pick $T_1 = T_{M,1}(\frac{\epsilon_1}{2})$ in order to account for turbocharger inertia (which drives the air flow dynamics).
2) We choose $\epsilon_2 > 0$ and use $T_2 = \max\{T_2 \in [T_m(T_1), T_{M,2}(T_1, \epsilon_2)] / \forall t \in \mathbb{R}^+ dist(u^{\text{mp}}(t), \mathcal{U}) < \epsilon_2\}$.

These rules guarantee that the constraints are not violated by more than $\max\{\epsilon_1, \epsilon_2\}$.

## V. Experimental results

### A. Tests setup

The proposed constrained motion planning control strategy was first tested in simulation. For that purpose, a high frequency engine model was developed in AMESim [9]. The combustion heat release model is based on the conventional 0D Diesel combustion model approaches [7], [4] extended to multi-pulse injection, and taking into account auto-ignition delay and EGR effect corrections. These changes were made for sake of accuracy over the whole range of operating set points, especially in both Highly Premixed Combustion (HPC) and conventional combustion modes (see [1] for more details). This model seems a good representation of the main phenomena of the engine and is an appropriate tool for control design. Its main purpose is tuning through an hardware in the loop approach. The same code can be kept from simulation to real-time application.

### B. Implementation

On the test bench, the global control scheme is implemented as summarized in Figure 4. The air path observer

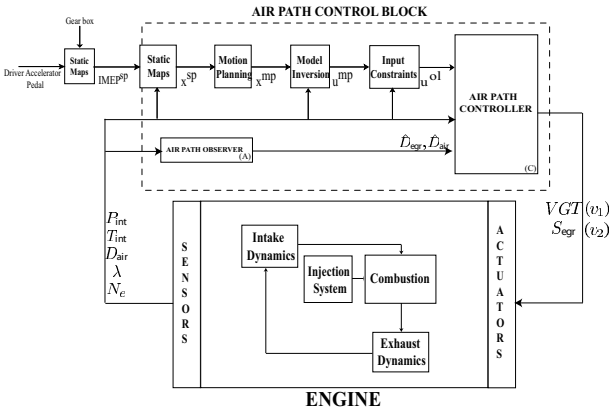


Fig. 4. Control Scheme

block (Block (A)) stands for the observer described in [6]. This block gives an estimation of the BGR and the EGR flow. The motion planning block implements the constrained motion planning open loop control strategy described in Section III. Eventually, fast monovariable controllers are added to the structure (Block (C)) to provide further accuracy and robustness. In details, a PI controller on the normalized EGR flow is used on the EGR valve. On the other hand, a PI controller on the air mass flow is used on the VGT. These controllers implicitly deal with flows upper bounds. In the case of input saturations, they eventually prevent steady state errors.

### C. Experimental results

Figures 5, 6 and 7 report experimental closed-loop results. The scenario is a varying torque demand at constant engine speed (1500 rpm) in both HCCI combustion mode and conventional combustion mode. We now detail these experiments.

*1) From $t = 102s$ to $t = 112s$:* here, we have an IMEP transient at 1500 rpm in HCCI combustion mode. The IMEP of the system starts at 2 bar and eventually reaches 5 bar. This transient aims higher intake pressure and BGR setpoints. Starting and ending operating points are both in HCCI combustion mode. Let us focus on Figure 5. By contrast with all decentralized controllers, we notice on that our controller takes into account the well known non minimum phase behavior of the system reported in [16]. More precisely, one can check that the main contribution to this is due to the open-loop controller (the closed loop control histories being very close to it). When the EGR valve opens, the flow increases leading to a pressure rise in the intake manifold. Meanwhile, the exhaust pipe acts as a discharge for the VGT. Its opening lowers the EGR supplied to the turbocharger yielding a significant drop of the exhaust manifold flow. The turbocharger slows down which eventually causes the decrease of the intake manifold

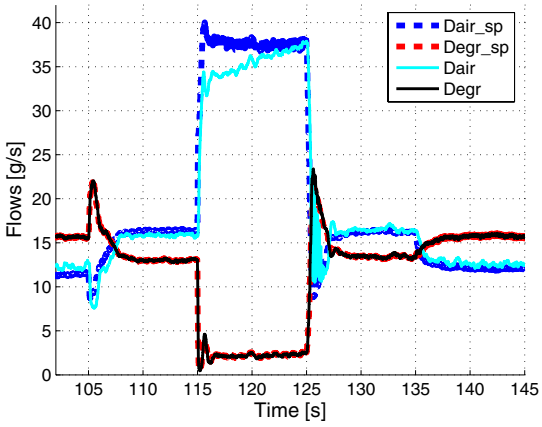


Fig. 5. Experimental results: IMEP transient from 2 to 5 bar, to 9 bar, to 5 bar, and then to 4 bar at 1500 rpm. Flow histories. Dashed : set point ($u^{sp}$), solid: closed-loop trajectory.

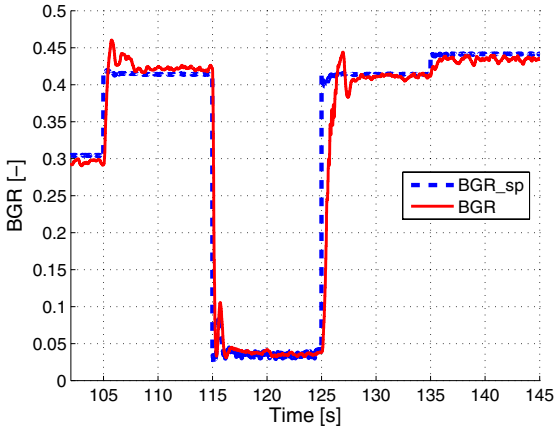


Fig. 6. Experimental results: IMEP transient from 2 to 5 bar, to 9 bar, to 5 bar, and then to 4 bar at 1500 rpm. BGR histories. Dashed : set point, solid: closed-loop trajectory.

pressure. This phenomenon is delayed and slowed down by the turbocharger inertia. Simple ramps and/or steps will fail to let the system reach the desired setpoint. With the proposed control strategy, the model takes into account this complex behavior. The motion planning efficiently drives the system to its setpoint.

*2) From $t = 112s$ to $t = 122s$:* here, we have a tip-in (high increase of torque demand) at 1500 rpm. Implicitly, it is desired to steer the system from a low load point with high EGR to a high load point with much less BGR. The proposed open loop control strategy successively closes the EGR valve and then closes the VGT with an overshoot. One can notice the resulting decrease in EGR flow and simultaneous increase of the fresh air flow. As expected from a motion planning control strategy, this does provide a soft landing for the state variables $x_1$ and $x_2$ onto their set points. During the transient, the open loop control laws are indeed saturated. This results in the temporary mismatch between the airflow and its set point. This effect is particularly noticeable on this very large

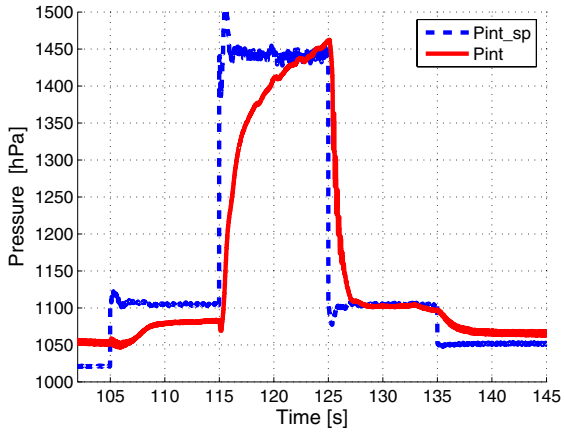


Fig. 7. Experimental results: IMEP transient from 2 to 5 bar, to 9 bar, to 5 bar, and then to 4 bar at 1500 rpm. Intake pressure histories. Dashed : set point, solid: closed-loop trajectory.

pressure transient that we choose for sake of illustration.

Again, transients are smooth and present only small oscillations. It is instructive to note that, in this exact same setup, we failed to get a decentralized controller preventing both stall and noises. The main reason for this seems the undesired overshoot of the BGR.

### *D. Performance analysis*

TABLE II

EXPERIMENTAL RESULTS FOR THE INTAKE PRESSURE TRANSIENT. $T_1$ IS THE REFERENCE TIME FOR THE MOTION PLANNING STRATEGY (TDC-TIME SCALE), $\mathcal{T}_1$ IS THE 5% ERROR CONVERGENCE TIME. N.C. STANDS FOR NOT CONVERGING BEFORE NEXT TRANSIENT STARTS.

| **IMEP [bar]** | **Pressure [bar]** | $T_1$ | $\mathcal{T}_1$ |
|---|---|---|---|
| $4 \rightarrow 5$ | $1.05 \rightarrow 1.11$ | 45 | 105 |
| $5 \rightarrow 6$ | $1.11 \rightarrow 1.11$ | 4 | 60 |
| $6 \rightarrow 7$ | $1.11 \rightarrow 1.29$ | 80 | 85 |
| $7 \rightarrow 9$ | $1.29 \rightarrow 1.44$ | 60 | n.c. |
| $8 \rightarrow 2$ | $1.35 \rightarrow 1.02$ | 90 | 110 |
| $2 \rightarrow 8$ | $1.02 \rightarrow 1.35$ | 90 | n.c. |
| $5 \rightarrow 9$ | $1.11 \rightarrow 1.44$ | 90 | n.c. |
| $9 \rightarrow 5$ | $1.44 \rightarrow 1.11$ | 90 | 123 |

Equations (10) and (12) serve as guidelines for tuning in this experiment. The parameters $T_1$ and $T_2$ were designed in simulation on the presented reference model. For experimental purpose, the control is done each Top-Down Center (TDC) and the reference motion planning (2) is implemented as a discrete filter. As it appears in simulation, a good rule-of-the-thumb is

$$\begin{cases} T_1 &= T_{0,1} + \Delta_1(sign(\bar{x}_1 - \underline{x}_1))\,|\bar{x}_1 - \underline{x}_1| \\ T_2 &= T_{0,2} + \Delta_2(sign(\bar{x}_2 - \underline{x}_2))\,|\bar{x}_2 - \underline{x}_2| \end{cases}$$

where $T_0$ is a constant and $\Delta$ is a function with only two possible values (switching when the reference is increasing or decreasing). Tuning is important to make open loop motion planning consistent with actual constraints. Tables II and III present the comparison between the expected transient times $T_1$ and $T_2$ (used for the motion planning strategy in (3), (6) (7), and (8)) and the observed convergence times (within 5%) $\mathcal{T}_1$ and $\mathcal{T}_2$. Interestingly, both are often very close, although in extreme cases (such as strong tip-in), the actual convergence time can be largely underestimated.

TABLE III

EXPERIMENTAL RESULTS FOR THE BGR. $T_2$ IS THE REFERENCE TIME FOR THE MOTION PLANNING STRATEGY (TDC-TIME SCALE), $\mathcal{T}_2$ IS THE 5% ERROR CONVERGENCE TIME.

| **IMEP [bar]** | **BGR [-]** | $T_2$ | $\mathcal{T}_2$ |
|---|---|---|---|
| $4 \rightarrow 5$ | $.44 \rightarrow .41$ | 20 | 42 |
| $5 \rightarrow 6$ | $.41 \rightarrow .24$ | 25 | 26 |
| $6 \rightarrow 7$ | $.24 \rightarrow .10$ | 24 | 24 |
| $7 \rightarrow 9$ | $.10 \rightarrow .04$ | 21 | 22 |
| $8 \rightarrow 2$ | $.08 \rightarrow .30$ | 65 | 42 |
| $2 \rightarrow 8$ | $.30 \rightarrow .08$ | 21 | 23 |
| $5 \rightarrow 9$ | $.41 \rightarrow .04$ | 21 | 21 |
| $9 \rightarrow 5$ | $.04 \rightarrow .41$ | 80 | 84 |

In summary, the results are good, even with a reasonably large transient. We are able to follow the planned trajectory. High pressure setpoint are more difficult to reach due to the turbocharger inertia and friction. However, it is not needed to accurately track the intake pressure because, for pollutant reduction purposes, only BGR needs to be closely controlled provided a limited Air-Fuel Ratio is guaranteed. The errors on the intake pressure will only lead to a very small error on the torque production. Nevertheless, on a vehicle, this problem will not appear because as the torque production increases, in response the engine speed and the turbocharger speed increases. This phenomenon is expected to be reduced in real-vehicle applications.

## VI. CONCLUSION

The presented work demonstrates the relevance of motion planning in the control of the –coupled– airpath dynamics of turbocharged Diesel engines using Exhaust Gas Recirculation. For the HCCI combustion mode, very large rates of burned gas need to be considered and we have proven on a realistic test-bench cases that the proposed approach can handle such situations. Despite strong coupling, the airpath dynamics has nice properties that make it easy to steer through our control strategy. Its triangular form yields exponential convergence over a wide range of setpoints. It can also be shown, through a simple analysis, to satisfy operational constraints, provided transient are chosen sufficiently smooth.

The next step will be to adapt the strategy to other engine configurations, i.e. two turbochargers and/or two EGR pipes with various thermal conditions.

*Acknowledgments:* The authors would like to thank Yann Creff for his support, Sébastien Potteau for providing the experimental facilities, and Antoine Albrecht for providing the engine model.

## REFERENCES

[1] A. Albrecht, J. Chauvin, S. Potteau, and G. Corde, "Design of real-time torque balancing control for highly premixed combustion engine using a 1D Diesel engine model," in *Proc. of the IAV Conference "Engine process simulation and supercharging"*, 2005.

[2] M. Ammann, N. Fekete, L. Guzzella, and A. Glattfelder, "Model-based control of the VGT and EGR in a turbocharged common-rail Diesel engine: theory and passenger car implementation," in *Proc. of the SAE Conference*, no. 2003-01-0357, 2003.

[3] P. Amnéus, D. Nilsson, F. Mauss, M. Christensen, and B. Johansson, "Homogeneous Charge Compression Ignition engine: Experiments and detailed kinetic calculations," in $4^{th}$ *International Symposium on Diagnostic and Modeling in Internal Combustion Engines*, 1998.

[4] C. Barba and C. Burkhardt, "A phenomenological combustion model for heat release rate prediction in high-speed DI Diesel engines with common rail injection," in *Proc. of the SAE Conference*, no. 2000-01-2933, 2000.

[5] J. Chauvin, G. Corde, N. Petit, and P. Rouchon, "Experimental motion planning in airpath control for HCCI engine," in *Proc. of the IEEE Conf. American Control Conference*, 2006.

[6] J. Chauvin, G. Corde, C. Vigild, N. Petit, and P. Rouchon, "Air path estimation on Diesel HCCI engine," in *Proc. of the SAE Conference*, no. 2006-01-1085, 2006.

[7] F. Chmela and G. Orthaber, "Rate of heat release prediction for direct injection Diesel engines based on purely mixing controlled combustion," in *Proc. of the SAE Conference*, no. 1999-01-0186, 1999.

[8] A. Hultqvist, U. Engdar, B. Johansson, and J. Klingmann, "Reacting boundary layers in a homogeneous charge compression ignition (HCCI) engine," in *Proc. of the SAE Conference*, no. 2001-01-1032, 2001.

[9] IMAGINE, *AMESim user manual, http://www.amesim.com*, 2004.

[10] M. Janković and I. Kolmanovsky, "Robust nonlinear controller for turbocharged Diesel engine," in *Proc. of the American Control Conference*, 1998.

[11] ——, "Constructive Lyapounov control design for turbocharged Diesel engines," *IEEE Transactions on Control Systems Technology*, vol. 8, pp. 288–299, 2000.

[12] M. Jung and K. Glover, "Control-oriented linear parameter-varying modelling of a turbocharged Diesel engine," 2003.

[13] ——, "Comparison of uncertainty parameterisations for H-infinity robust control of turbocharged Diesel engines," vol. 13, pp. 15–25, 2005.

[14] J. Kahrstedt, K. Behnk, A. Sommer, and T. Wormbs, "Combustion processes to meet future emission standards," in *Motortechnische Zeitschrift*, 2003, pp. 1417–1423.

[15] M. Kao and J. Moskwa, "Turbocharged Diesel engine modelling for nonlinear engine control and estimation," *ASME Journal of Dynamic Systems, Measurements and Control*, vol. 117, 1995.

[16] I. Kolmanovsky, A. Stefanopoulou, P. Moraal, and M. van Nieuwstadt, "Issues in modelling and control of intake flow in variable geometry turbocharged engines," in *Proc of the $18^{th}$ IFIP Conference on System Modelling and Optimization*, 1997.

[17] M. B. Milam, "Real-time optimal trajectory generation for constrained systems," Ph.D. dissertation, California Institute of Technology, 2003.

[18] A. Stefanopoulou, I. Kolmanovsky, and J. Freudenberg, "Control of variable geometry turbocharged Diesel engines for reducted emissions," *IEEE Transactions on Control Systems Technology*, vol. 8, pp. 733–745, 2000.

[19] M. van Nieuwstadt, I. Kolmanovsky, P. Moraal, A. Stefanopoulou, and M. Janković, "Experimental comparison of EGR-VGT control schemes for a high speed Diesel engine," *Control System Magazine*, vol. 20, pp. 63–79, 2000.

[20] M. van Nieuwstadt, P. Moraal, I. Kolmanovsky, A. Stefanopoulou, P. Wood, and M. Criddle, "Decentralized and multivariable designs for EGR-VGT control of Diesel engine," in *Proc of the $2^{nd}$ IFAC Workshop on Advances in Automotive Control*, 1998.

[21] B. Walter and B. Gatellier, "Near zero $NO_x$ emissions and high fuel efficiency diesel engine: the NADI$^{TM}$ concept using dual mode combustion," vol. 58, no. 1, pp. 101–114, 2003.